International Geology Review, Vol. 46, 2004, p. XXX–XXX.

Fast Cooling and Exhumation of the Valhalla Metamorphic Core Complex, Southeastern British Columbia

FRANK S. SPEAR

Department of Earth and Environmental Sciences, Rensselaer Polytechnic Institute, Troy, New York 12180

Abstract

High-grade, migmatitic paragneisses (820°C, 8 kbar peak conditions) of the Valhalla metamorphic core complex experienced the retrograde net transfer reaction (ReNTR):

garnet + melt + K-feldspar = sillimanite + biotite + plagioclase

during cooling and crystallization of the melt, resulting in an increase in the Fe/(Fe + Mg) of both garnet and biotite at their margins. Diffusion profiles generated by this increase in Fe/(Fe + Mg) have been modeled numerically. Optimal fits were obtained with an initial, short period of rapid cooling (> 200°C/m.y. for < 0.5 m.y.) followed by slower (but still rapid) cooling at 20–30°C/m.y. for 10–20 m.y.

Four generations of monazite have been observed. Monazite inclusions within garnet contain only generations 1 and 2, and generations 3–4 are found only in matrix monazites. Generations 1–2 record ages of 75–85 Ma, which is believed to be represent the prograde metamorphism of the complex. A single age of ~105 Ma may represent an early contact metamorphic episode. Third-generation monazite is 60 ±2 Ma, and reflects near-peak conditions. Generation 4 monazite, which occurs only on the outer rims of monazite, has not been dated, but is believed to represent monazite produced during melt crystallization. A hornblende K-Ar age of 58±2 Ma suggests a cooling rate of several tens to several hundreds of degrees/Ma immediately following the metamorphic peak.

The extremely rapid cooling (hundreds of degrees/m.y.) at ~60 Ma must have been tectonically induced and it is suggested that transport of the hot Valhalla complex onto cooler basement up a thrust ramp along the underlying Gwillim Creek shear zone was the cause. Two-dimensional thermal modeling indicates that thrust transport of several centimeters/year up a 20° ramp will produce the observed cooling rates. The subsequent slower cooling rate (tens of degrees/m.y.) is believed to have been the result of extensional unroofing by low-angle normal faulting along the Slocan Lake fault.

Introduction

THIS CONTRIBUTION examines the cooling history of the Valhalla complex based on a new interpretation of the origin of chemical zoning observed on the rims of garnet in paragneisses from the central part of the complex. In a previous contribution (Spear and Parrish, 1996), the petrologic cooling rate was constrained by models in which diffusion was driven only by retrograde Fe-Mg exchange reaction (ReER) between biotite and garnet; the exchange reaction mechanism was ensured by examining only inclusions of biotite within garnet. In this contribution, the implications of retrograde net transfer reaction (ReNTR) on the garnet rim composition and resultant diffusional zoning is modeled. The cooling rate required to match the garnet rim zoning pattern is considerably faster than previously believed (over 100°C/Ma), and a 2-D thermal model involving significant tectonic shortening along a thrust ramp prior to the onset of extension is presented as a probable explanation. The proposed rapid cooling is supported by new, in situ dates on monazite, which constrain the shortening event to have occurred over a very short time period (less than 1 Ma) at ~60 Ma. These results are entirely consistent with the conclusions of Spear and Parrish (1996) and Schaubs et al. (2002), who suggest cooling of the complex was controlled by thrusting onto a cold footwall.

Geologic Setting and Petrology

The Valhalla complex (Fig. 1) is one of several metamorphic core complexes in the Shuswap terrane of eastern British Columbia and vicinity. The complex (Fig. 1) is comprised of Cretaceous orthogneisses, Paleocene–Eocene granitoids, and paragneisses of unknown depositional age. The complex

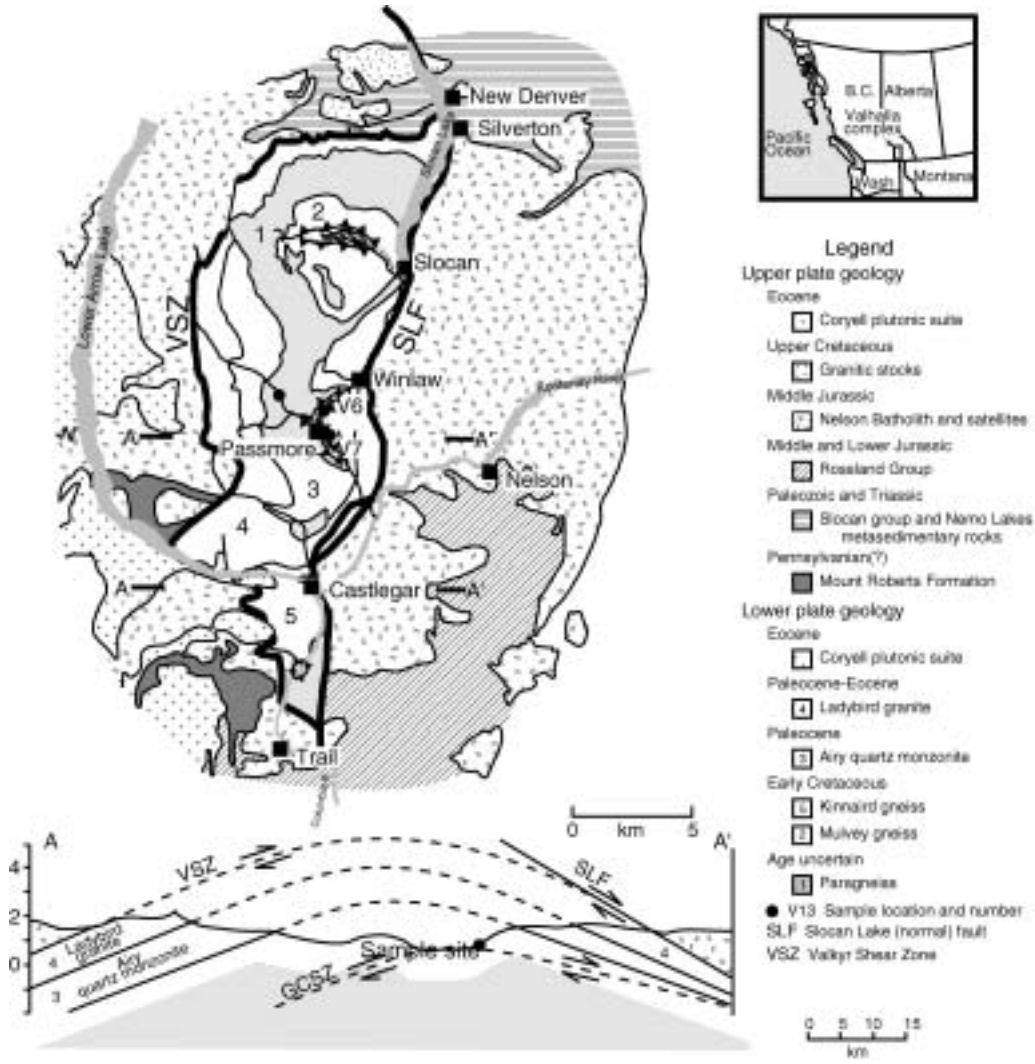

FIG. 1. Geological map of the Valhalla complex showing the location of samples described in this study (V6 and V7). Inset shows location of map in southeastern British Columbia. The lower panel shows a cross section along line A-A'. Note the proximity of the samples to the overhanging Slocan Lake fault and underlying Gwillim Creek Shear Zone (GCSZ).

is bounded on the east by the Slocan Lake low-angle normal fault and on the north, west, and south by the Valkyr shear zone, both with shear indicators indicating top down to the east. The complex is floored by the Gwillim Creek shear zone, which occurs at the deepest exposed structural levels throughout the complex. A Lithoprobe traverse across the complex identifies the Gwillim Creek shear zone as a major crustal reflector (Cook et al., 1988).

Paragneisses of the Valhalla complex experienced peak metamorphic conditions of approximately 820°C, 0.8 GPa at 65–75 Ma (Fig. 2; see also Spear and Parrish, 1996; Schaubs et al., 2002). Exhumation of the complex commenced at ~57 Ma (Carr et al., 1987) by low-angle normal faulting along the Valkyr shear zone and the Slocan Lake fault. The average cooling rate during this exhumation is well constrained by several geochronologic

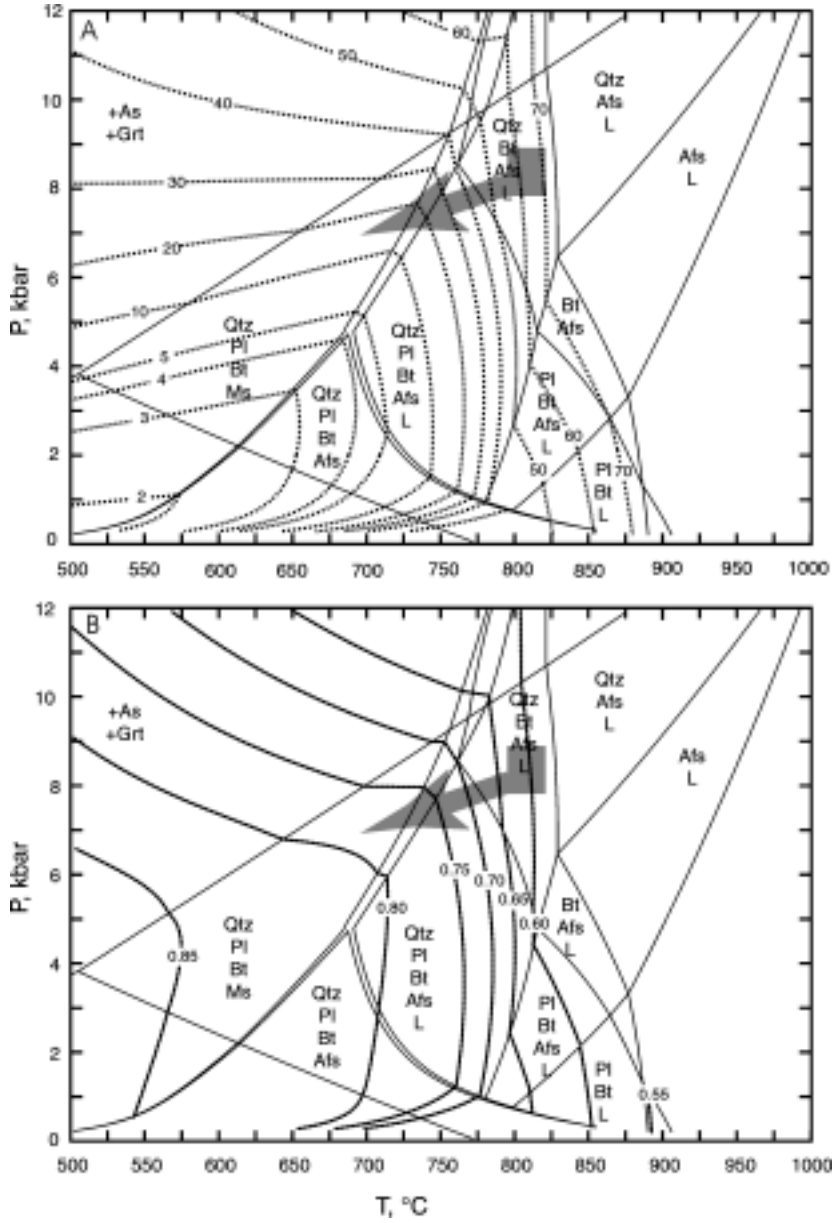

FIG. 2. P-T pseudosection (stability diagram) for a typical paragneiss bulk composition. Fields are labeled with stable mineral assemblages (all assemblages contain Al_2SiO_5 + garnet). The peak P-T conditions and retrograde P-T path are shown in gray. A. Diagram contoured for garnet abundance (millimoles garnet/100 cm^3 of rock). B. Diagram contoured for Fe/(Fe+Mg) in garnet. Note that along the retrograde P-T path (gray arrow), garnet is consumed and the Fe/(Fe+Mg) of the remaining garnet increases.

systems to around 25°C/m.y. (Carr et al., 1987; Parrish et al., 1988, Parrish, 1995; Spear and Parrish, 1996).

The samples selected for detailed study (V6B and V7C) are from the Passmore gneiss. The location of the samples with respect to major faults and

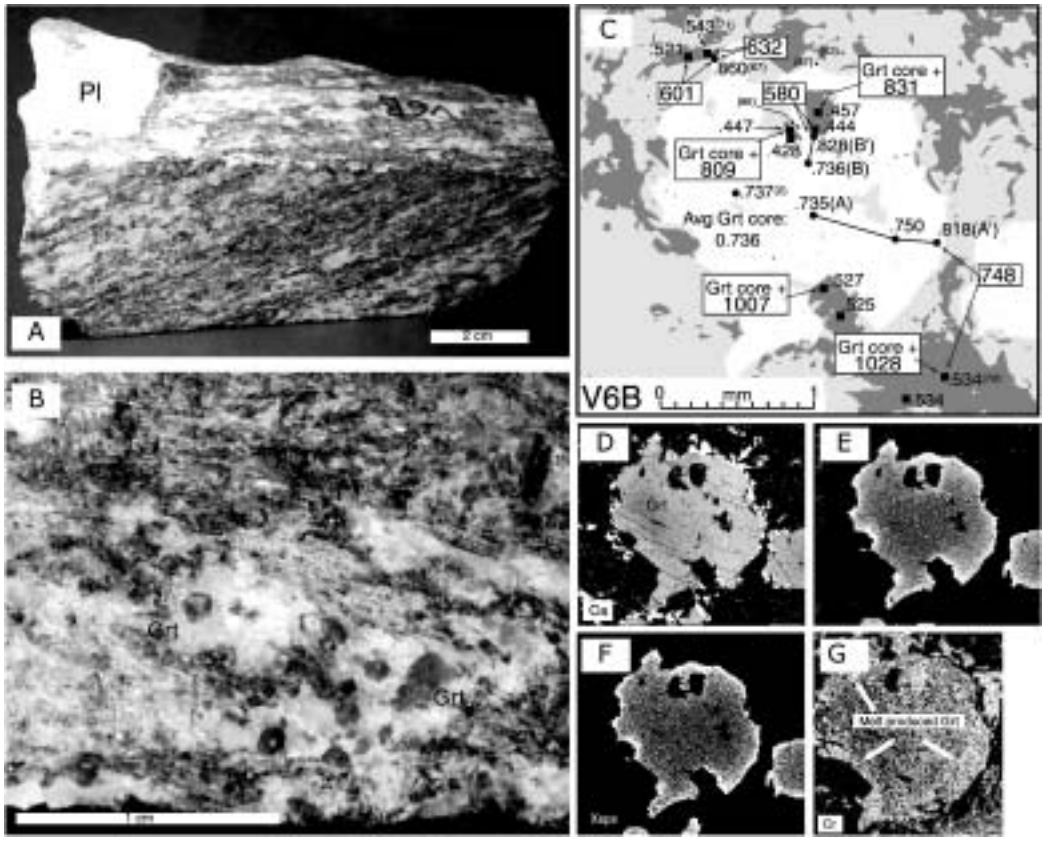

FIG. 3. A and B. Hand sample photographs of migmatite from sample V6B. Note garnet-bearing pods of leucosomes in B. C. Sketch of part of a thin section from sample V6B showing Fe/(Fe + Mg) of garnet and biotite (dark grey). Numbers in boxes are temperatures calculated from Fe-Mg exchange thermometry based on analyses from the garnet and biotite spots indicated. Note that the temperature obtained from the garnet core + matrix biotite is in excess of 1000°C (peak T ~820°C) and the temperature obtained from the garnet rim + matrix biotite is 748°C (the T at which reaction 1r ceased). D–G. X-ray maps of garnet shown in (C) showing zoning in Ca (D), Fe/(Fe + Mg) (E), Mn (F), and Cr (G). Ca and Cr zoning are growth zoning; Cr zoning shows the part of the garnet produced from prograde reaction 1. Fe/(Fe + Mg) and Mn zoning are diffusion zoning; the Mn zoning is evidence that the ReNTR (1r) has consumed garnet during cooling.

shear zones is important for the thermal modeling presented later and warrants discussion. The samples are located within domain P-I of Schaubs et al. (2002), within and immediately above highly sheared migmatites that are interpreted as splays of the Gwillim Creek shear zone. The samples are also located approximately four kilometers beneath the Slocan Lake fault (Fig. 1 cross section; see also Schaubs et al., 2002).

Reaction History

A pseudosection depicting the stable mineral assemblages for a paragneiss similar to those of the Valhalla complex is shown in Figure 2, contoured for moles of garnet (Fig. 2A) and Fe/(Fe + Mg) in garnet (Fig. 2B). The calculated P-T conditions are well within the field for dehydration melting, and paragneisses from the Valhalla complex contain abundant leucosomes (Fig. 3A). Garnet is found in both melanosomes and leucosomes (Fig. 3B), indicating that at least some garnet grew by the reaction

$$\text{sillimanite} + \text{biotite} + \text{plagioclase} + \text{quartz} = \text{garnet} + \text{melt} + \text{K-feldspar}, \quad (1)$$

consistent with the garnet molar isopleths (Fig. 2A). Spear and Parrish (1996) identified the parts of

garnet that had grown by reaction 1 as having higher Ca than the garnet cores (Figs. 3B and 5B). The Ca zoning in Figure 3D is a bit ambiguous, but is interpreted as reflecting growth zoning based on other samples. The Cr zoning (Fig. 3G) clearly shows a rim of higher Cr, which is interpreted as garnet produced by reaction 1.[1] Fe, Mg, and Mn display only diffusional zoning (Figs. 3E and 3F).

There is strong evidence in these paragneisses for progress of both the retrograde net transfer reactions (ReNTR)

garnet + melt + K-feldspar =
sillimanite + biotite + plagioclase + quartz (1r)

and the retrograde exchange reaction (ReER)

pyrope + annite = almandine + phlogopite. (2r)

ReER (2r) is especially obvious around inclusions of biotite within garnet (e.g., Fig. 3E), where the Fe/(Fe+Mg) increases toward the inclusion. Evidence for reaction (1r) operating in a retrograde sense comes from several sources, as indicated below.

1. Garnets are embayed on their margins (e.g., Figs. 3D, 3E, and 4), consistent with crossing the garnet molar isopleths along the retrograde path shown in Figure 2A.

2. Zoning of elements that display growth zonation (e.g., Ca and Cr) is truncated (e.g., Figs. 3D and 3E).

3. Fe, Mg, and Mn zoning is symmetric around garnet (c.f. Tracy et al., 1976).

4. Mn is zoned at the garnet rim, indicating garnet resorption.

5. ReNTR products (sillimanite + biotite + plagioclase + quartz) are concentrated at the garnet rim. This can be seen in Figure 3D where plagioclase decorates the upper right-hand side of the garnet crystal. Figure 4 displays ReNTR products, including quartz + plagioclase symplectite at the garnet rim.

6. Thermometry using garnet core and matrix biotite results in temperatures significantly higher than the peak temperature (i.e., over 1000°C; Fig. 3C). This occurs because matrix biotite is driven toward more Fe-rich compositions as a result of the ReNTR.

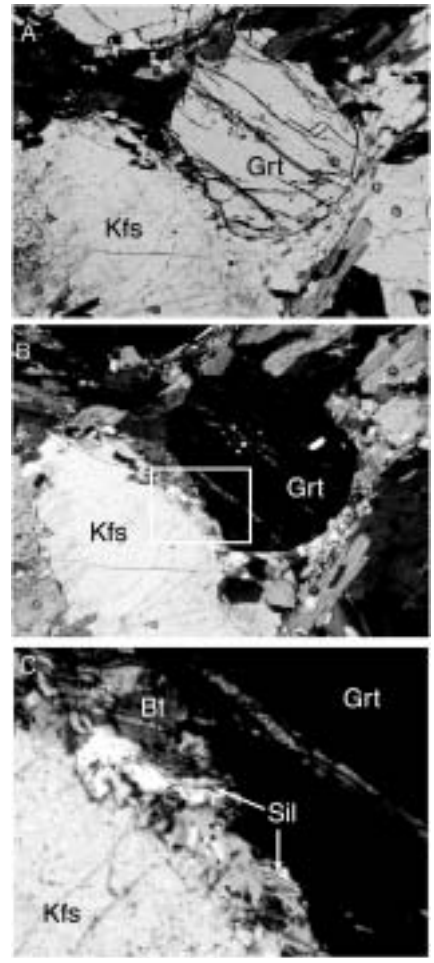

FIG. 4. Sample V6B; photomicrographs of textures produced by ReNTR 1r. A. Garnet rim is resorbed everywhere adjacent to matrix. B. Same view as (A) in crossed polars. Box shows location of (C). C. Close-up view (crossed polars) showing sillimanite + biotite + quartz + plagioclase symplectite produced along the garnet rim by operation of ReNTR 1r.

7. Garnet Fe/(Fe + Mg) increases towards the rim, consistent with the isopleths in Figure 2B, and biotite also becomes more Fe-rich as the garnet rim is approached. This zoning is consistent with a ReNTR but not a ReER.

In summary, biotite inclusions within garnet experienced only retrograde Fe-Mg exchange with enclosing garnet. In contrast, the rims of most garnets in sillimanite-bearing paragneisses are zoned as the result of diffusion driven by compositional

[1]See Spear and Kohn, 1996, for discussion of the partitioning arguments for this zoning behavior.

changes on the garnet rim caused by the retrograde net transfer reaction (1r).

A comparison of the zoning profiles produced by ReNTR (1r) and ReER (2r) is shown in Figure 5. Although broadly similar, zoning produced by ReER (2r) has a slightly shorter penetration distance for Fe/(Fe+Mg), and does not show significant Mn zoning at the boundary. Another significant difference is that locally biotite modified by ReER (2r) becomes more Mg-rich towards the adjacent garnet, whereas biotite affected by ReNTR (1r) becomes more Fe-rich toward garnet. It should be pointed out that on the garnet rim where ReNTR (1r) was operative, equilibrium described by ReER (2r) was also maintained, the significant point being that the boundary composition was controlled by both reactions 1r and 2r acting together. The significance of identifying the correct retrograde reaction history for diffusion modeling will be discussed in more detail below.

Gwillim Creek shear zone. The timing of the deformation along the Gwillim Creek shear zone is important for the tectonic history discussed below, so evidence that relates the movement along the shear zone to the rock history is critical. A photomicrograph showing the texture of a sample from locality 6 (sample V6E) was presented by Spear and Parrish (1996, Fig. 8). The onset of shearing relative to onset of ReNTR (1r) is constrained by the presence of biotite produced by this reaction in the pressure shadows of deformed garnets (Fig. 8C in Spear and Parrish, 1996). Therefore, some deformation must have occurred before ReNTR (1r) went to completion.

The cessation of shearing relative to the ReNTR is constrained by the following observations. Sillimanite and biotite produced by the ReNTR (1r) are aligned in the shear fabric, some leucosomes produced by the ReNTR are aligned in the foliation, and garnet is broken and has a sigmoid shape. These observations indicate that deformation continued after some progress on the ReNTR had occurred. Cessation of major shearing in sample V6E must have occurred before or soon after the final completion of reaction (1r) because the garnet diffusion zoning produced in response to reaction (1r) is not disrupted. Biotite adjacent to garnet (Figs. 8B and 8C in Spear and Parrish, 1996) is zoned with higher Fe/Mg closest to the garnet, indicating that little or no retrograde Fe-Mg exchange occurred after cessation of reaction (1r). Garnet-biotite exchange thermometry on the garnet-biotite pair in closest proximity (adjoining rim analyses) yields 713°C (Hodges and Spear, 1982 calibration), indicating that this is the temperature of cessation of reaction (1r). Not coincidentally, this is also the approximate temperature of the solidus in this sample, suggesting that reaction (1) ceased when the last melt crystallized. Consequently, shearing must have ceased at a temperature slightly below the solidus. In summary, the available evidence suggests that shearing on the Gwillim Creek shear zone was more or less coincident with progress of ReNTR (1), and that shearing ceased at conditions near the solidus.

Diffusion Modeling

Since the pioneering study of Lasaga et al. (1977), a number of papers have used diffusion modeling of zoning in garnet to constrain the cooling history of metamorphic rocks. To the author's knowledge, all of these studies with the exception of Spear and Florence (1992) assumed Fe-Mg exchange to be the reaction responsible for the changing boundary concentration on the garnet rim that drove diffusion. As discussed above, ReER (2r) was the only reaction that operated between biotite inclusions and enclosing garnet, but ReNTR (1r) (with ReER 2r) operated between the garnet rim and the matrix, and is responsible for the diffusive zoning on the garnet rim.

The significance of this difference for diffusion modeling can be seen in the T-X section of Figure 6A. Garnet rim compositions change along two different T-X paths, depending on the reaction(s) that are operative. Specifically, the Fe/(Fe + Mg) of garnet rim changes much more gradually (dX/dT is smaller) if ReER (2r) is the only reaction operating. For example, consider the T-X curves in Figure 6A starting at a peak temperature of 820°C and a garnet with a core Fe/(Fe + Mg) of 0.645 and a hypothetical rim Fe/(Fe + Mg) of 0.78. If only ReER (2r) has operated on the garnet rim, then the rim composition would not be realized until the temperature reaches < 500°C. In contrast, if ReNTR (1r) has operated, the garnet rim composition is realized when the temperature reaches ca. 760°C.

The effect on the diffusion modeling can be seen in Figure 6B. A cooling rate of 100°C/m.y. generates a diffusion penetration distance of ~400 μm with the ReNTR as the boundary condition, whereas the same cooling rate with the ReER as the boundary condition only generates a penetration distance of 100 μm or so. Consequently, attempts to model a

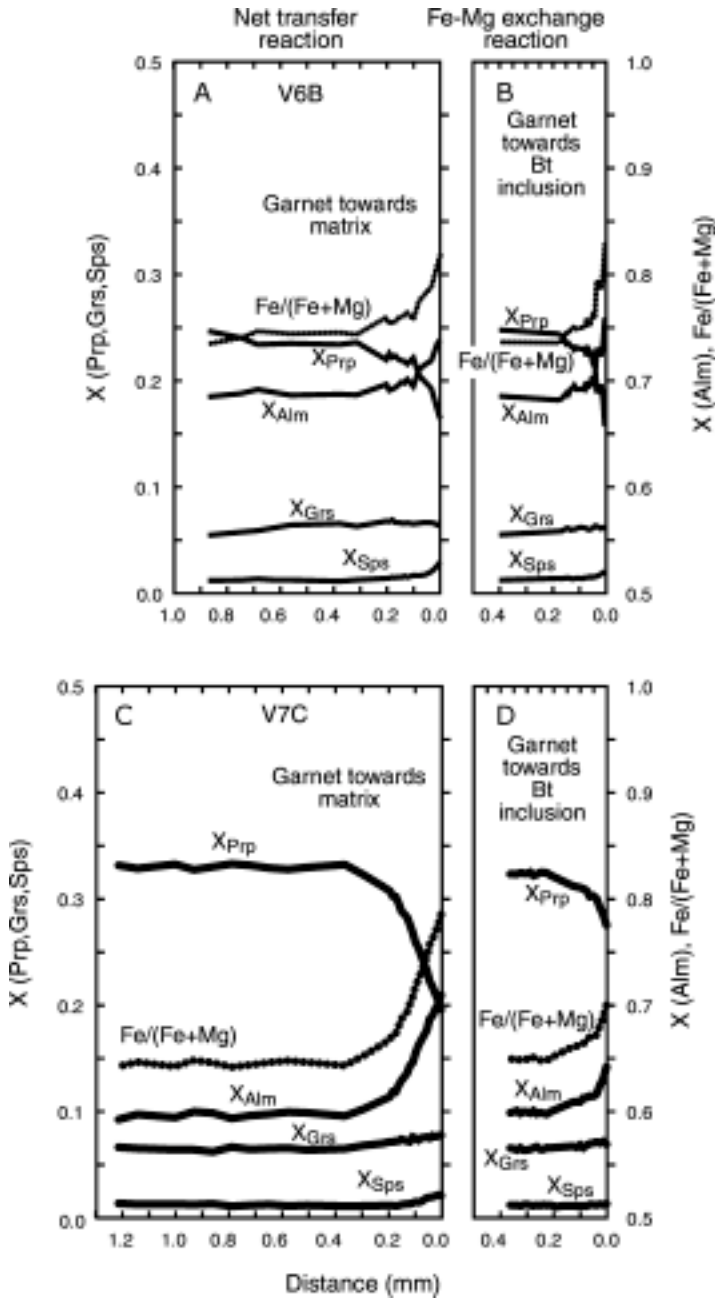

FIG. 5. Line traverses showing garnet zoning from samples V6B (A, B) and V7C (C, D). A and C. Core to rim traverses. Note upturn of Mn on the garnet rim toward the matrix, indicating that ReNTR 1r has operated at this interface. B and D. Traverse toward a biotite inclusion within garnet. Note the absence of significant increase in Mn toward the biotite inclusion, indicating that only ReER 2r has been operative at this interface.

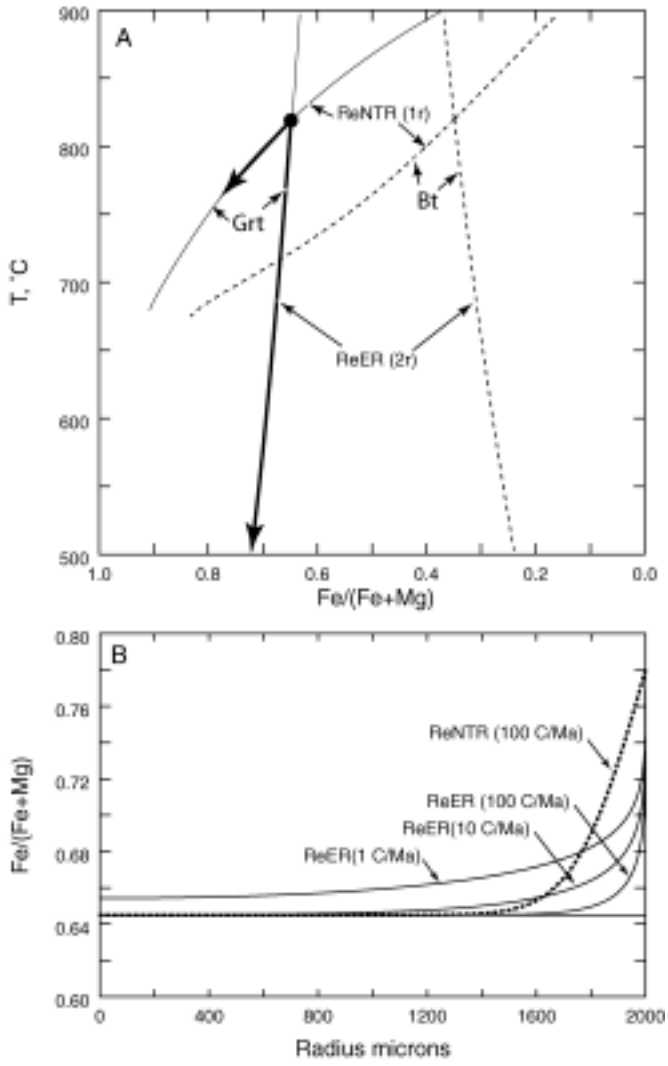

FIG. 6. A. T-X diagram (P = 8 kbar) showing how the Fe/(Fe + Mg) in garnet (solid lines) and biotite (dashed lines) change with temperature based on the ReNTR 1r and the ReER (2r). Note that dX[Fe/(Fe + Mg)]/dT is significantly larger for the ReNTR than for the ReER. B. Plot of Fe/(Fe + Mg) versus distance from garnet rim, showing calculated diffusion profiles assuming a ReNTR boundary condition with a cooling rate of 100°C/m.y. (dotted line) and a ReER boundary condition at three different cooling rates (solid lines). Note the difference in the shapes of the profiles, and the marked difference in diffusion penetration distance.

particular zoning profile using a ReER as the boundary condition will always result in a significantly slower cooling rate than modeling the same profile using a ReNTR as the boundary condition.

Based on the above discussion, it is clear that correct assignment of the boundary condition governing reaction (ReNTR versus ReER) is one of the most critical factors in modeling garnet zoning profiles. The problem can be abstracted somewhat by realizing that the key factor is the temperature at which the boundary condition is set—i.e., the T-X trajectory of the garnet rim.

Constraints on the T-X path of a garnet rim that is governed by a ReER are relatively straightforward because the exchange reaction can be used to calculate the garnet rim composition based on the ΔH of

reaction and mass balance assumptions (i.e., how much biotite is present in the sample) (Lasaga et al., 1977; Lasaga, 1983). Figure 6A shows the exchange reaction T-X path for sample V7C calculated for the garnet-biotite exchange thermometer. The path is nearly linear, and suggests that the garnet rim composition around biotite inclusions (where only ReERs are operative) was set at less than 600°C.

Constraints on the T-X path of a garnet rim that is governed by a ReNTR can be obtained by: (a) thermodynamic modeling of the T-X behavior of the inferred governing reaction (e.g., Figs. 2A and 6A); (b) direct measurement of the temperature at which the rim composition was set using thermometry; and (c) inferences based on phase equilibria considerations. Thermodynamic modeling of sample V7C (Fig. 6A) indicates that the rim Fe/(Fe + Mg) was reached at a temperature of approximately 760°C. The garnet rim–matrix biotite temperature yielded by this sample is 709°C (see Fig. 5D of Spear and Parrish, 1996) and the solidus temperature is ~710°C.[2] Thermodynamic modeling of sample V6B (not shown) suggests the rim Fe/(Fe + Mg) was established at ~785°C; the garnet-biotite temperature for the garnet rim/matrix biotite is 748°C (see Fig. 4D of Spear and Parrish, 1996) and the solidus temperature is again ~710°C. The approach taken here will be to model the garnet rim zoning using the extremes of the boundary T-X constraints, which will yield a maximum and minimum cooling rate for each sample.

Results

An explicit finite difference diffusion model (written in FORTRAN) was used for all calculations. The program is designed so that the T-X path of a garnet rim composition can be specified as starting and ending T-X points, with intermediate compositions calculated by linear interpolation. Linear cooling rates are used. Several attempts at modeling the zoning profiles using a single cooling rate resulted in poor fits; therefore, a strategy of breaking the T-t history into a number of linear segments with different cooling rates was adopted, with significantly improved fits. Diffusivities of Chakraborty and Ganguly (1992) were used for all calculations.

Results of the diffusion models are shown in Figures 7 and 8 and Table 1. As discussed above, the cooling rates required to match the diffusion profiles are particularly sensitive to the T-X relation for the garnet rim. To explore the range of possible cooling rates, two models of the ReNTR were run for each sample. The first uses the highest temperature estimate for the establishment of the rim boundary condition (i.e., 785°C and 762°C for V6B and V7C, respectively), which comes from the calculated T-X diagram (e.g., Fig. 6). The second ReNTR model assumes that the final rim condition was not set in until the solidus was reached at approximately 710°C. The first ReER models used the temperature inferred from the calculated T-X diagram (e.g. 440°C and 550°C, Fig. 6) and the second models were based on calculated garnet-biotite temperatures along mutual contacts in the sample (e.g. 550°C and 582°C).

Because the garnet rim composition controlled by the ReNTR "freezes in" at high temperature, it is the high-temperature cooling history that is most sensitive to the ReNTR diffusion models. Similarly, the ReER freezes in at lower temperature, and it is this part of the T-t history that is most sensitive to the ReER diffusion models.

The high-temperature T-t histories determined for each of the four ReNTR models are relatively similar (Fig. 8A). Each shows an initial pulse of rapid cooling followed by more gradual cooling to ca. 40 Ma. The cooling rates required to match the zoning profiles vary somewhat (Fig. 8B), but are all in excess of 200°C/m.y. One model (V6B ReNTR 785) requires a cooling rate of 1000°C/m.y. for approximately 0.1 Ma to achieve a good fit.

The lower temperature T-t histories as constrained by the ReERs are similar to each other (dashed lines in Fig. 8A), but reflect somewhat slower cooling than suggested by models of the ReNTRs. Indeed, the cooling rates inferred from the ReERs are inconsistent with the available geochronology (dots in Fig. 8A), and with the rocks being at ambient temperature at the surface today. The reason for this is unknown, but the only way to increase the cooling rate over this interval using the same diffusivities is to increase the temperature at which the garnet rim temperature was "frozen." Values of approximately 650°C yield cooling rates of ~25°C/m.y., consistent with the geochronology.

Discussion

Spear and Parrish (1996) presented results of a diffusion model in which only biotite inclusions within garnet were modeled, restricting the type of retrograde reaction to the garnet-biotite Fe-Mg

[2]Note that the ReNTR requires the presence of melt so the solidus is the lower T limit.

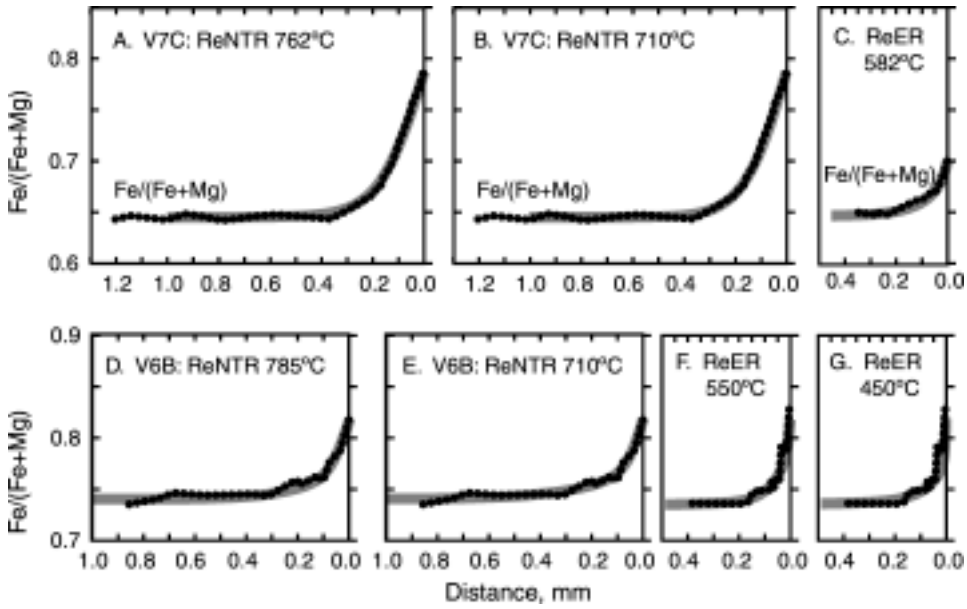

FIG. 7. Plots of Fe/(Fe + Mg) versus garnet radius (distance in mm) showing measured Fe/(Fe + Mg) zoning profiles (dotted lines) and diffusion model fits (solid lines). A–C. Sample V7C. D–G. Sample V6B. Each model begins at 820°C with a homogeneous garnet and assumes a different T-X (or X-t) path for the boundary condition (Fe/(Fe + Mg) in garnet). Models (A), (B), (D), and (E) assume the ReNTR boundary condition and models (C), (F), and (G) assume the ReER boundary condition. In all cases, the rim garnet Fe/(Fe + Mg) is attained at the temperature indicated in the panel.

ReER (2r). Best-fit cooling rates based on these calculations were ~25°C/m.y. (range of 3–80°C/m.y.) for rocks from the same locality studied here and using the same diffusivities (Chakraborty and Ganguly, 1992). These values are completely consistent with the cooling rates obtained for ReERs in the present study.

Ducea et al. (2003) also modeled the zoning on the rim of garnet from sample V7C and obtained a cooling rate of 2–13°C/m.y. based on the assumption that the garnet rim composition was controlled by ReER (2r). This result is consistent with the modeling presented here, but our present interpretation of the garnet rim is that it was controlled by ReNTR (1r), and the initial cooling rate should be 1–2 orders of magnitude faster.

Geochronology

Age dating

Monazite occurs in a number of textural settings in migmatites from the Valhalla complex. Figure 9A shows a BSE image of a paragneiss containing two large garnet crystals. Monazite is located both inside garnet (grain 4) and in the matrix (grains 3 and 5).

Chemical zoning (especially Y) is different in each of the texturally distinct monazites (Figs. 9C–9E), and at least four distinct generations of monazite have been identified based on the Y zoning. Monazite inside of garnet (grain 4; Fig. 9B) is comprised of high- and low-Y zones (zones 1 and 2, respectively). The same high- and low-Y patches (zones 1 and 2) can be seen in the monazites in the matrix (grains 5 and 3; Figs. 9C–9D). Matrix monazites have an additional zone outboard from zones 1 and 2 that contains the lowest Y values (zone 3), and locally tips on grains that are intermediate Y (zone 4). Pyle and Spear (2003) documented four generations of monazite growth in samples of similar metamorphic grade from central New Hampshire.

In situ ages were obtained using the IMS 1270 ion microprobe at Woods Hole Oceanographic Institute and UCLA. Procedures were the same as those discussed by Spear et al. (2004). The Pb/Th ages are reported here.

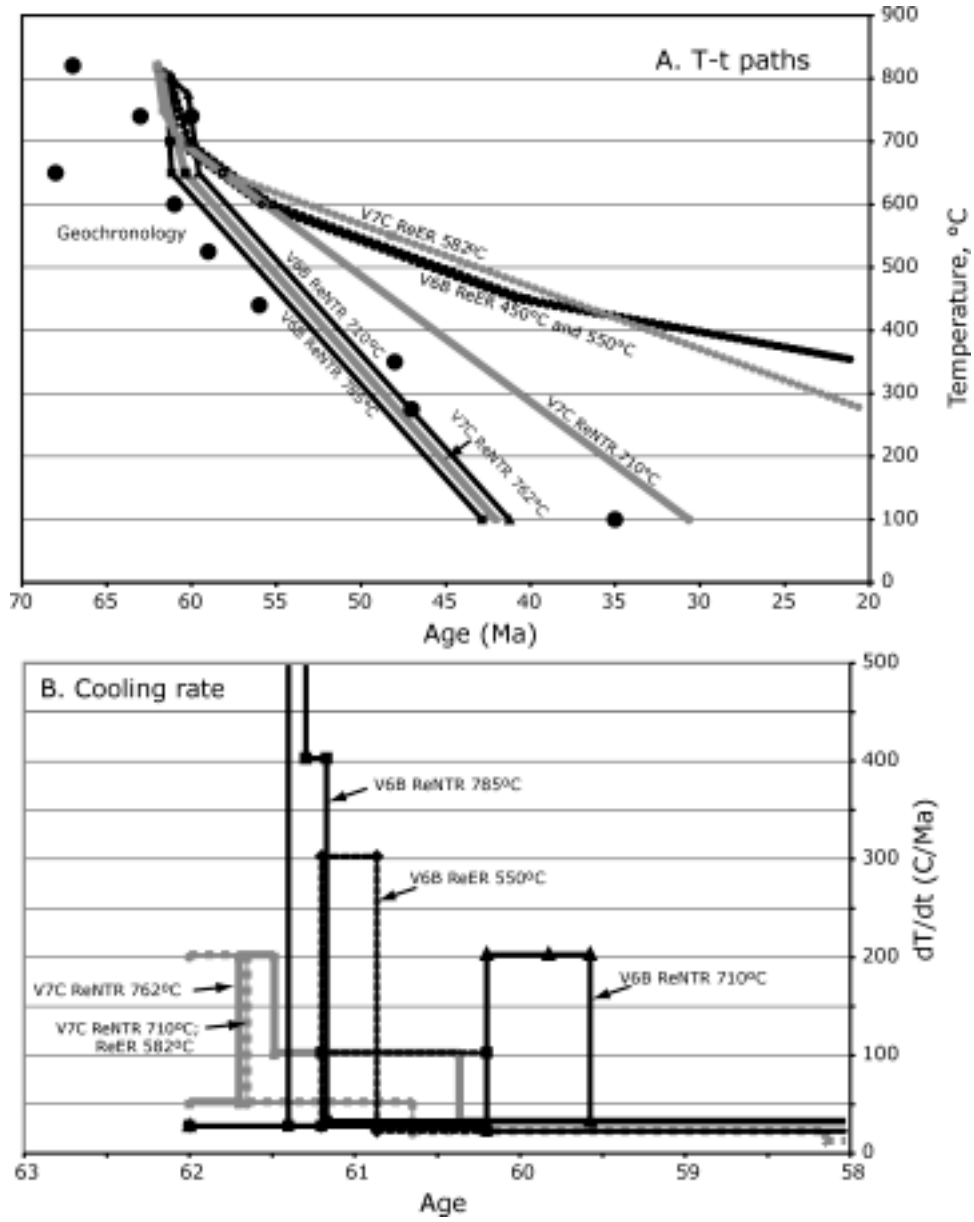

FIG. 8. Summary of results of diffusion models. A. T versus t plot. B. dT/dt versus t plot. Each curve is one of the diffusion models shown in Figure 7. Solid lines are models with ReNTR boundary conditions and dotted lines are models with ReER boundary conditions. Dots in (A) are T-t constraints from geochronology. Note that the ReER models give cooling rates that are slower than those assuming ReNTR boundary condition, and are not consistent with cooling rates from geochronology.

Zone 1–2 monazite ages span the range 75–85 Ma (Fig. 9). Although the statistical uncertainty in the ages (ca. ± 1 Ma) is smaller than the spread, the relative uncertainties must be larger owing to effects other than counting statistics (e.g., sample charging), so it is concluded that zone 1–2 ages are distinguishable.

The age of zone 3 monazite is significantly younger (~60 Ma) and, unfortunately, no zone 4

TABLE 1. T-t Histories and Cooling Rates Used in Diffusion Models

	T	t, m.y.	DT/dt
	V6B		
ReNTR 785	820	0.00	
	805	0.60	25
	700	0.11	1000
	650	0.13	400
	100	18.33	30
ReNTR 710	820	0.00	
	775	1.80	25
	700	0.38	200
	650	0.25	200
	100	18.33	30
ReER 550	820	0.00	
	800	0.80	25
	700	0.33	300
	600	5.00	20
	450	15.00	10
	100	70.00	5
ReER 450	820	0.00	
	800	0.80	25
	700	1.00	100
	600	5.00	20
	450	15.00	10
	100	70.00	5
	V7C		
ReNTR 762	820	0.00	
	805	0.30	50
	762	0.22	200
	650	1.12	100
	100	18.33	30
ReNTR 710	820	0.00	
	750	0.35	200
	700	1.00	50
	650	2.50	20
	100	27.50	20
ReER 582	820	0.00	
	750	0.35	200
	700	1.00	50
	650	2.50	20
	550	10.00	10
	100	45.00	10

monazite was dated. Based on comparison with the study of Pyle and Spear (2003), in which monazites from similar rocks are well characterized in terms of their paragenesis, the zone 4 monazite is interpreted to have grown during melt crystallization. Zone 4 monazite must, therefore, represent monazite that was produced either during or prior to melting reactions. It also requires that melt crystallization occurred later than approximately 60 Ma.

Discussion of age data

An extensive amount of geochronology has been done on the Valhalla complex (e.g., Parrish 1995; Parrish et al, 1988; summarized in Spear and Parrish, 1996 and Schaubs et al., 2002), much of which is multigrain TIMS analyses of monazite. The complex zoning displayed by the monazites examined in this study suggest that many of the previous analyses may represent mixed domains. There is no evidence in the Y zoning that diffusion has homogenized Y contents during peak metamorphism, and similar studies have revealed no Pb diffusional zoning (e.g., Crowley and Ghent, 1999). Therefore, it is inferred that the previous multi-grain TIMS ages on monazite are mixed, and do not reflect Pb loss (e.g., Harrison et al., 2002).

Spear and Parrish (1996) argued from these earlier data that the metamorphic peak in the Valhalla complex occurred at 67–80 Ma. The present results, on the other hand, indicate that cooling of the leucosomes could not have occurred until after ~60 Ma, and that anatexis may have been progressing as late as ~60 Ma.

A recent Sm-Nd age on the core and rim of garnet from sample V7C (Ducea et al., 2003) yielded 67.3 ± 2.3 for the core and 59.8 ± 2 Ma for the rim. Ducea et al. (2003) assumed that the peak metamorphic age was close to the core 67.3 Ma determination and that the rim age of 59.8 reflected Nd loss during relatively slow cooling of a few degrees C/m.y. Slow cooling from the metamorphic peak is inconsistent with the diffusion calculations presented here. However, it is entirely possible that slow cooling did occur between ca 67 and 60 Ma followed by a pulse of rapid cooling.

Thermal/Tectonic Model for Rapid Cooling of the Valhalla Complex

The diffusion modeling discussed above indicates that the zoning observed on garnet rims required a very rapid episode of cooling from the

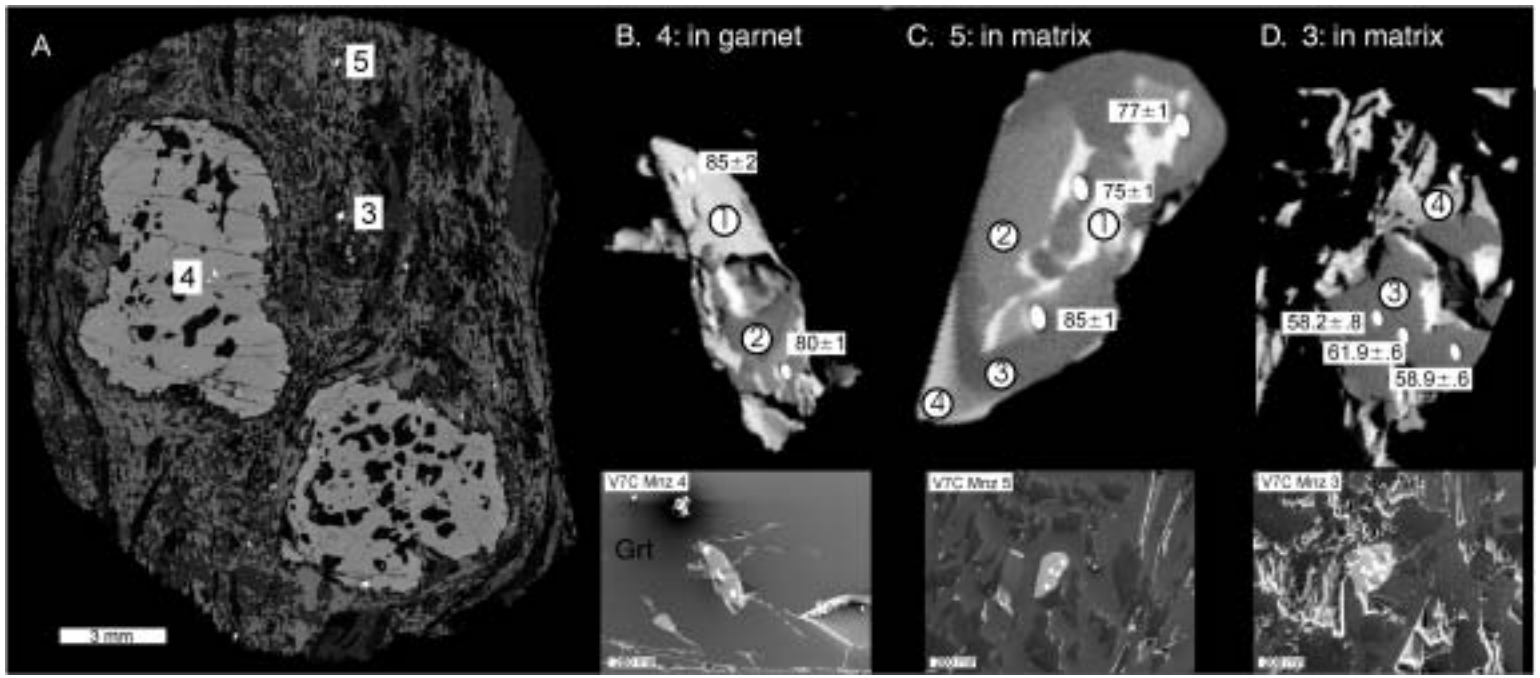

FIG. 9. Sample V7C. A. BSE image showing location of analyzed monazite crystals in sample. B–D. Upper panels are yttrium X-ray maps depicting the distribution of Y in analyzed monazites. Numbers in circles are monazite growth zones (1–4) based on Y zoning. Lower panels are SE images showing location of SIMS analysis spots (white ellipses). Ages are shown in boxes in the upper panels.

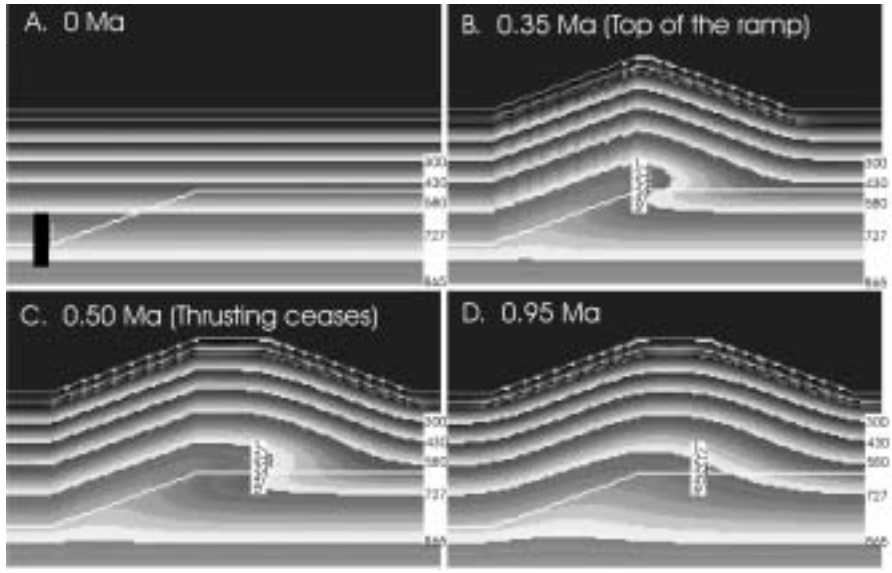

FIG. 10. Cross sections showing the evolution of two-dimensional thermal model with a 20° thrust ramp. Transport velocity is 10 cm/year for 0.5 m.y. Note the thermal overhang in (C). Temperatures of isotherms are given on the right side of each panel. Numbered dots (1–5) refer to rocks for which paths are plotted in Figure 11.

metamorphic peak during melt crystallization in order to preserve the zoning. Furthermore, in situ geochronology indicates that the crystallization of leucosomes did not begin until after ~60 Ma, thereby greatly compressing the time available to achieve cooling of the complex.

Rapid cooling at rates constrained by this study is only possible by mechanisms that involve tectonic juxtaposition of rocks of different temperature. Erosion as a means of cooling rocks (e.g., England and Richardson, 1977; England and Thompson, 1984) is limited by the thermal diffusivity of rocks and length scales involved (tens of kilometers of crust) and a maximum of a few tens of degrees/Ma is possible by this mechanism.

Tectonic denudation by normal faulting provides a mechanism for rapid exhumation and cooling of a core complex, and the Slocan Lake low-angle normal fault was certainly a major factor in the exposure of the Valhalla complex during the early Tertiary. However, the Slocan Lake fault cannot be responsible for the initial, very rapid cooling of the paragneisses for two reasons. First, rapid cooling of footwall rocks will only occur in rocks immediately below the fault. Rocks farther from the fault will cool more slowly as thermal conduction permits. The samples discussed here are 4 km structurally below the Slocan Lake fault, and would not, therefore, have cooled at the rates observed. Second, and most convincingly, exhumation by faulting results in P-T paths of footwall rocks that would first show nearly isobaric unloading, followed by cooling. The rocks of the Valhalla complex display no evidence whatsoever for decompression during cooling; rather the post-peak P-T path is nearly isobaric cooling (e.g., Fig. 2), thus ruling out the possibility that the Slocan Lake fault was responsible for the initial rapid cooling observed.

One possible explanation of the rapid cooling is that it was the result of transport of hot, high-grade rocks of the Valhalla complex up a thrust ramp onto a cooler footwall, which provided the heat sink for cooling the complex, as suggested by Spear and Parrish (1996) and Schaubs et al. (2002). Such a mechanism would result in nearly isobaric cooling paths, as observed. The rate of cooling would be determined by the rate of transport, the thrust ramp angle, the lateral thermal gradient (if any), and the proximity of the rocks in the hanging wall to the heat sink below the fault. Indeed, Schaubs et al. (2002) provide evidence that rocks closer to the Gwillim Creek shear zone cooled more rapidly than those farther away, consistent with this "footwall quenching" model.

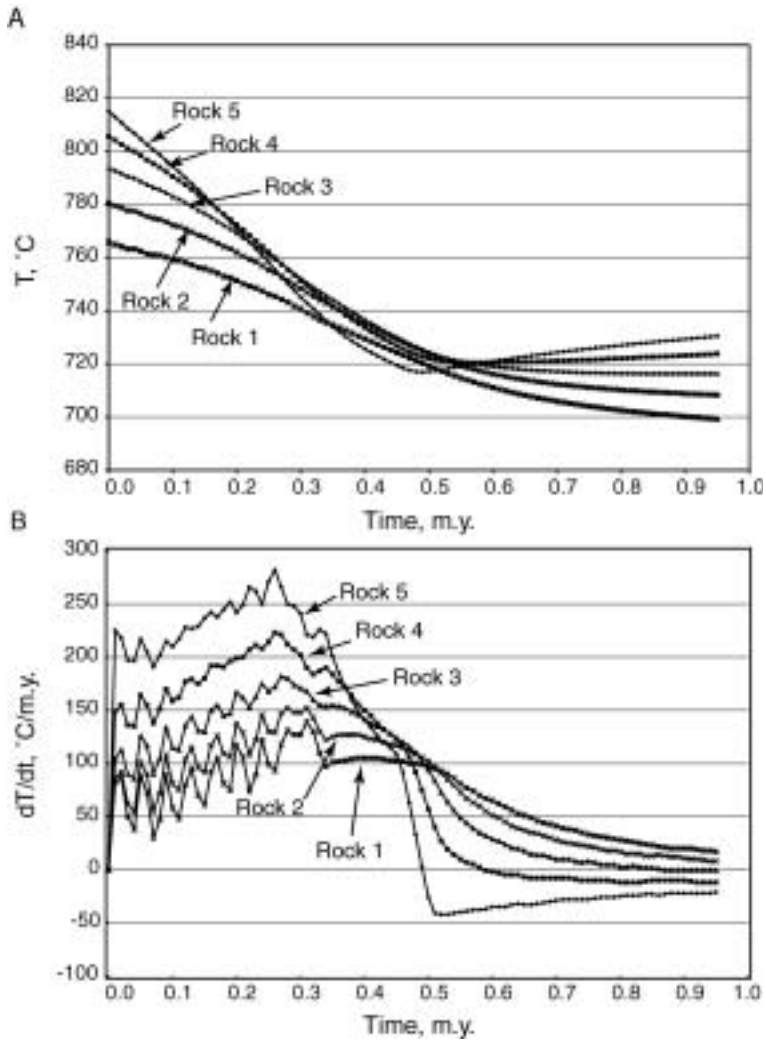

FIG. 11. Plots of (A) temperature versus time and (B) cooling rate versus time for the five rocks shown in the 2-D thermal model in Figure 10 at distances of 4.5, 3.5, 2.5, 1.5, and 0.5 km from the fault (rocks 1–5, respectively). Note that cooling rates of all rocks within 4 km of the fault are in excess of 100°C/m.y.

In order to determine whether this mechanism could produce the calculated cooling rates given reasonable input parameters, a two-dimensional thermal model was invoked (Fig. 10). The most important model parameters for determining the cooling rate are the thrust velocity and the ramp angle: the steeper the ramp and the faster the thrust rate, the faster the rocks will cool. Several models were examined in detail and a representative one with a ramp angle of 20° and a thrust velocity of 10 cm/year are shown in Figures 10 and 11. Thrusting at 10 cm/year up a 20° ramp results in a thermal overhang, as can be seen in Figures 10B and 10C, which then decays with time (Fig. 10D). Slower thrusting rates (e.g., 5 cm/year) or gentler ramps (e.g. 10° dip) do not produce thermal overhangs, but still produce rapid cooling.

Results are also shown in T versus t and dT/dt versus t plots (Fig. 11) for five rock positions located as shown in Figure 10 (4.5, 3.5, 2.5, 1.5, and 0.5 km above the thrust). Cooling is most rapid in rock 5 (located 0.5 km from the thrust) and for this model

(10 cm/year; 20° ramp) rock 5 cools in excess of 200°C/m.y. Even rocks several km from the thrust ramp (e.g., rock 1) cool in excess of 100°C/m.y. Note that there is a major inflection in the temperature-time plots (Fig. 11A) at the time in which thrusting ceases. Indeed, the rock closest to the fault (Rock 5) cools initially but then heats up for the duration of the model (to 1 m.y.) after thrusting ceases. This is a consequence of thermal relaxation following the formation of the thermal overhang (Figs. 10C and 10D). Late heating following thrusting is not suspected to have happened in the Valhalla complex because unroofing due to normal faulting and erosion will have mitigated this effect. However, such a phenomenon might be manifest in some terranes above thrust faults, resulting in differing P-T paths over short distances with no intervening structures.

The cooling-rate plots (Fig. 11B) show two inflections. The major inflection occurs at 0.5 m.y. when thrusting ceased (note that the cooling rate for Rock 5 becomes negative as the rock heats up). A second inflection occurs at ~0.35 m.y. when the rocks reach the top of the thrust ramp (Fig. 11B).

Additional models have been run to examine the range of possible thrust ramp angles and thrust velocities. For example, a thrust velocity of 2 cm/year up a 20° ramp results in cooling rates of ~70–80°C/m.y.; a thrust velocity of 10 cm/year up a 10° ramp results in cooling rates of 60–100°C/m.y. Because of the wide range of calculated cooling rates for the Valhalla complex (~100–1000°C/Ma), it was not deemed appropriate to attempt to fit the thermal history of the complex any more accurately than has been presented. The goal of this exercise was to demonstrate that with reasonable geological parameters, cooling rates of several hundreds of degrees/m.y. are expected. Based on the above thermal models, a thrust rate of several cm/year or faster up a thrust ramp of 10 degrees or more will produce the observed cooling rates greater than 100°C/m.y.

Discussion

Rapid cooling of the Valhalla complex through quenching by emplacement on a cool footwall ramp was argued by both Spear and Parrish (1996) and Schaubs et al. (2002); post-metamorphic juxtaposition of units of different metamorphic histories is also reported from the Monashee complex (Crowley and Parrish, 1999). This paper presents the first direct evidence that the cooling rate was in excess of 100°C/m.y., virtually requiring a thrust-ramp mechanism.

This is the period of Late Cretaceous shortening in the Omenica belt. The reason for such rapid thrust emplacement may be directly tied to the presence of melt in the Valhalla paragneisses. Hollister and Crawford (1986) suggested that major deformations might be significantly enhanced by the presence of melt (anatexis), and the petrology and geochronology of the Valhalla complex is consistent with this model. It is also probably no coincidence that deformation on the Gwillim Creek shear zone apparently ceased when the rocks cooled through the solidus. Indeed, it is entirely possible that the timing and amount of shortening in the Late Cretaceous was controlled by the existence of melt in the middle crust. Once the melt crystallized, further shortening was not possible and strain was partitioned elsewhere.

Extremely rapid cooling as has been documented here is not believed to be unique to the Valhalla complex. Other examples of high-grade garnets with similar diffusion zoning have been described in the literature and, based on the discussion here, are probably the result of net transfer reaction rather than exchange reaction as was assumed. If so, then based simply on the similarity of diffusion penetration distance of Fe/(Fe + Mg) in garnet from these samples, the cooling rates of these other samples must have been quite rapid. It is possible that rapid thrusting and subsequent quenching of migmatite terranes is a common phenomenon.

Acknowledgments

The author wishes to thank J. T. Cheney for invaluable insights during many late night discussions on the interpretation of pelitic schist phase equilibria and monazite geochronology. T. Mark Harrison and Graham Layne provided necessary access to and assistance with the SIMS analyses reported here. X-ray maps of monazite were collected by J. Pyle. Insightful and constructive reviews were provided by S. Carr and J. Ganguly.

REFERENCES

Carr, S. D., Parrish, R. R., and Brown, R. L., 1987, Eocene structural development of the Valhalla complex, southeastern British Columbia: Tectonics, v. 6, p. 175–196.

Chakraborty, S., and Ganguly, J., 1992, Cation diffusion in aluminosilicate garnets—experimental determination

in spessartine-almandine diffusion couples, evaluation of effective binary diffusion coefficients, and applications: Contributions to Mineralogy and Petrology, v. 111, p. 74–86.

Cook, F. A., Green, A. G., Simony, P. S., Price, R. A., Parrish, R. R., Milkereit, B., Gordy, P. L., Brown, R. L., Coflin, K. C., and Patenaude, C., 1988, Lithoprobe seismic reflection structure of the southeastern Canadian Cordillera: Initial results: Tectonics, v. 7, p. 157–180.

Crowley, J. L., and Ghent, E. D., 1999, An electron microprobe study of the U-Pb-Th systematics of metamorphosed monazite: The role of Pb diffusion versus overgrowth and recrystallization: Chemical Geology, v. 157, p. 285–302.

Crowley, J. L., and Parrish, R., 1999, U-Pb isotopic constraints on diachronous metamorphism in the northern Monashee complex, southern Canadian Cordillera: Journal of Metamorphic Geology, v. 17, p. 483–502.

Ducea, M. N., Ganguly, J., Rosenberg, E. J., Patchett, P. J., Cheng, W., and Isachsen, C., 2003, Sm-Nd dating of spatially controlled domains of garnet single crystals: A new method of high temperature thermochronology: Earth and Planetary Science Letters, v. 213, p. 31–42.

England, P. C., and Richardson, S. W., 1977, The influence of erosion upon the mineral facies of rocks from different metamorphic environments: Journal of the Geological Society of London, v. 134, p. 201–213.

England, P. C., and Thompson, A. B., 1984, Pressure-temperature-time paths of regional metamorphism, Part I: Heat transfer during the evolution of regions of thickened continental crust: Journal of Petrology, v. 25, p. 894–928.

Harrison, T. M., Catlos, E. J., and Montel, J.-M., 2002, U-Th-Pb dating of phosphate minerals, *in* Kohn, M. J., Rakovan, J., and Hughes, J. M., eds., Phosphates: Geochemical, geobiological, and materials importance: Mineralogical Society of America, Reviews in Mineralogy and Geochemistry, no. 48, p. 523–558.

Hodges, K. V., and Spear, F. S., 1982, Geothermometry, geobarometry and the Al_2SiO_5 triple point at Mt. Moosilauke, New Hampshire: American Mineralogist, v. 67, p. 1118–1134.

Hollister, L. S., and Crawford, M. L., 1986, Melt-enhanced deformation—a major tectonic process: Geology, v. 14, p. 558–561.

Lasaga, A. C., 1983, Geospeedometry: An extension of geothermometry, *in* Saxena, S. K., ed., Kinetics and equilibrium in mineral reactions: New York, NY, Springer-Verlag, p. 81–114.

Lasaga, A. C., Richardson, S. M., and Holland, H. D., 1977, The mathematics of cation diffusion and exchange between silicate minerals during retrograde metamorphism, *in* Saxena, S. K., and Bhattacharji, S., eds., Energetics of geological processes: New York, NY, Springer-Verlag, p. 354–387.

Parrish, R., 1995, Thermal evolution of the southeastern Canadian Cordillera: Canadian Journal of Earth Sciences, v. 18, p. 944–958.

Parrish, R. R., Carr, S. D., and Parkinson, D. L., 1988, Eocene extensional tectonics and geochronology of the southern Omineca belt, British Columbia and Washington: Tectonics, v. 7, p. 181–212.

Pyle, J. M., and Spear, F. S., 2003, Four generations of accessory phase growth in low-pressure migmatites from SW New Hampshire: American Mineralogist, v. 88, p. 338–351.

Schuabs, P. M., Carr, S. D., and Berman, R. G., 2002, Structural and metamorphic constraints on ~70 Ma deformation of the northern Valhalla complex, British Columbia: Implications for the tectonic evolution of the southern Omineca belt: Journal of Structural Geology, v. 24, p. 1195–1214.

Spear, F. S., Cheney, J. T., Pyle, J. M., Harrison, M., and Layne, G., 2004, Monazite geochronology on a transect across central New England: Journal of Petrology, in review.

Spear, F. S., and Florence, F. P., 1992, Thermobarometry in granulites: Pitfalls and new approaches: Journal of Precambrian Research, v. 55, p. 209–241.

Spear, F. S., and Kohn, M. J., 1996, Trace element zoning in garnet as a monitor of crustal melting: Geology, v. 24, p. 1099–1102.

Spear, F. S., and Parrish, R., 1996, Petrology and petrologic cooling rates of the Valhalla Complex, British Columbia, Canada: Journal of Petrology, v. 37, p. 733–765.

Tracy, R. J., Robinson, P., and Thompson, A. B., 1976, Garnet composition and zoning in the determination of temperature and pressure of metamorphism, central Massachusetts: American Mineralogist, v. 61, p. 762–775.